Theoretical and Experimental Work on Optimal Contact Geometries on Fast Mechanical Disconnect Switches

T. Damle, L. Graber Georgia Institute of Technology

Abstract—Fast mechanical disconnect switches (FMS) are an integral part of hybrid circuit breakers, which are proposed as protection devices to clear faults in medium voltage distribution systems. The proposed FMS is a vacuum switch that is operated by an amplified piezoelectric actuator. Such actuators unprecedented speed and contact separation in less than one millisecond. The limitations that come with such designs are the low contact separation of typically less than one millimeter in open position and low contact force in the order of 100 N in closed position. This requires a new design of the contacts to operate under such constraints. The geometry of the contacts must be carefully designed to minimize electrical resistance when closed and minimize electric field enhancement when open. The paper presents finite element analysis and experimental results with the aim of identifying the most suitable contact geometry for FMS. The experiments show that optimized contact geometries have up to 40% less resistance than the initial spherical geometry.

Index Terms—Disconnector, Electrical Contact, Fault Current Limitation, Hybrid Circuit Breaker, Piezoelectric Actuator.

I. INTRODUCTION

The fault current levels in the electric grid is expected to increase with increase in distributed generation and DC systems [1, 2]. Interconnecting substations to increase the reliablity and resiliency of the distribution system also increases the fault current levels. The hybrid circuit breaker – which combines fast, low loss protection and fault current limitation – is increasingly proposed for protection of distribution systems that suffer under excessive fault current levels. Hybrid circuit breakers are a combination of solid state switch and a fast mechanical disconnect switch (FMS) connected in parallel, where the mechanical switch provides a low loss path during normal operation and the solid state switch (a semiconductor device) breaks the fault current.

While most of the research on hybrid circuit breaker technology has focused on different topologies of power electronic circuits [3] for breaking fault current and its operation in tandem with the FMS [4], work on the design of FMS is rather limited with two variants: Those base on Thompson coil actuators [5] and those based on amplified piezoelectric actuators (AMA) [6]. The FMS faces unique constraints such as sub-millimeter contact separation when open and high current carrying capability and limited contact force when closed. The optimal design of electric contacts is

essential for the FMS to work satisfactorily under these constrains.

The electric of contacts of the FMS should have a contact geometry that results in nearly uniform electric field (no field enhancement) to minimize the risk of electric breakdown when the contacts are open. Also, the contacts should have low power loss, which requires the contacts to have low bulk and constriction resistance. This requires careful selection of the material and geometry of the contact. This paper explores different contact geometries for the proposed design of the FMS, consisting of a switchgear paddle housing the AMA, the contacts, and the conductors, all in a vacuum switching chamber [7, 8, 9].

The proposed FMS is rated 15 kV and 600 A continuous current and has two ceramic bushings that act as electrical and thermal terminals on top of the grounded vacuum chamber. The piezoelectric actuator has an elliptical shell that amplifies the mechanical response. The shell is housed in a polymeric frame to which the outer conductors and the contact tabs are attached. The polymer of choice is polyether ether ketone (PEEK) due to its exceptionally low outgassing rate, low water absorption, and high glass transition temperature. The actuator is controlled by charging and discharging its electrostatic capacitance. The wires pass through a multi-pin feedthrough so that they can be interfaced from outside the vacuum chamber. The electric contacts of the FMS has spherical contacts of 5 mm radius, which have a maximum separation of 0.5 mm when they are open. This paper explores different contact geometries of Bruce and Rogowski shape [10, 11, 12, 13], which are used to make electrodes for applications that require uniform electric fields. Also considered are Ernst and Chang profiles [14, 15, 16], which were developed to produce uniform electric field to obtain glow discharge in TE gas lasers. Elliptical and flat contacts are also studied for the sake of comparison. The electric field across the gap and contact resistance is compared for all these geometries using finite element models and experiments. To approximate the contacts of the proposed FMS, all the studied contacts have a circular base of 5 mm diameter and a contact travel distance of 0.5 mm.

II. CONTACT GEOMETRIES

The section gives an overview of the different contact geometries considered in this paper. It gives details on the mathematical functions of these geometries and the selection of function parameters. All the geometries (except cylindrical contacts with flat tops) are shown in the half-plane. The three-dimensional contact geometry can be obtained by revolving this half plane around its z-axis by 360 degrees.

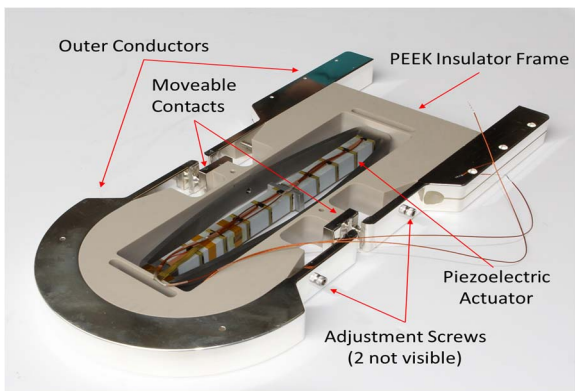




Fig. 1. Picture of the switch paddle of fast mechanical disconnect switch (top); CAD model and picture of the complete switch assembly (bottom left); Picture of the disconnect switch with feedthroughs (bottom right) – patent pending [8].

A) Flat Geometry

The electrical contacts are in the shape of a cylinder with the circular faces of the two contacts facing each other. This contact geometry is studied for comparison purposes only.

B) Spherical Geometry

The spherical geometry has one variable, the radius, and is given by the equations

$$x = Rcos(\theta) + x_c$$

$$y = Rsin(\theta) + y_c$$

where R is the radius, x_c and y_c are the coordinates of the center point, and θ is swept over $0 \le \theta \le \frac{\pi}{2}$.

C) Elliptical Geometry

The radius and the height can be controlled independently. It is given by the equations

$$x = a\cos(\theta) + x_c$$

$$y = bsin(\theta) + y_c$$

where a and b are the radius and height of the contact respectively.

D) Rogowski Geometry

The Rogowski geometry has two sections: an exponential and a circular section that make a smooth transition. The geometry was derived by calculating the electric field associated with a flat plane above and infinite ground plane. The exponential section of the geometry is defined by the equations [10,11,13].

$$x = \frac{A_r}{\pi} (\phi + e^{\phi} \cos \psi)$$

$$y = \frac{A_r}{\pi} (\psi + e^{\phi} \sin \psi)$$

where ϕ is the electrostatic line of force, ψ is the equipotential surfaces and A_r is the distance separating the flat plane and the ground plane. This can be assumed to be the distance of separation between the contacts and the Rogowski geometry can be drawn for a given distance of separation. The transition between circular and exponential section takes place at $\phi=0$. To ensure smooth transition between circular and exponential section, the coordinates of the center of the circle are calculated to be

$$x_c = -\frac{A_r}{\pi}$$

$$y_c = \frac{A_r}{\pi} (\frac{(1 + \cos\psi)^2}{\sin\psi} + \sin\psi + \psi)$$

The circular section ends at the point where the slope becomes vertical. The computer program used to generate the geometry can identify the end point.

E) Bruce Geometry

The Bruce geometry has three sections: a circular section, a sinusoidal section and a plane section. The contact geometry is drawn similar to the Rogowski profile with the circular section acting as the end points when it's slope gets vertical and the plane section completely eliminated. The sinusoidal section is expressed by the equation [11, 12, 13].

$$y = -R_e \sin(\frac{x}{X_0} \frac{\pi}{2})$$

To ensure smooth transition between circular and sinusoidal sections, R_e and X_0 are given by

$$X_0 = \frac{A_B}{\cos \alpha}$$

$$R_e = \frac{2}{\pi} X_0 tan\alpha$$

where α is the characteristic angle of the sinusoidal section. A_B is the distance separating the flat plane from the ground plane.

F) Chang Geometry

To construct the Chang geometry, two complex planes z = x + iy and W(z) = U + iV are defined where U is the flux function and V is the potential function. The analytical function is given by the equation [14,16].

$$z = W + KsinhW$$

where K is a constant that can be chosen arbitrarily and a different curve is generated for each value of K. The corresponding flux and potential function in the z-plane are given by the equations

$$x = U + K cos V sinh U$$

$$y = V + KsinVcoshU$$

To construct the geometry, the value of V is selected to be $\frac{\pi}{2} + \theta$, where θ is a variable and the values of x and y are calculated by sweeping the variable U from 0 to a point where the slope of the curve becomes vertical. So the Chang geometry is

controlled by 2 variables: θ and K and does not depend on the distance of separation between the contacts. The Chang geometry results in more compact contacts than Bruce or Rogowski geometry. Since all the contacts studied here have a radius of 5 mm, the Chang contacts have a flat section at its center, which gives more area of contact when the contacts are closed.

G) Ernst Geometry

The Ernst geometry results in a more compact geometry than the Chang geometry. The analytical function is given by [15,16].

$$z = W + k_0 sinhW + k_1 sinh2W + k_2 sinh3W$$

where k_0 , k_1 and k_2 are constants chosen arbitrarily and z and W are two complex planes similar to the Chang geometry. The corresponding flux and potential function in the z plane are given by the equations

$$x = U + k_0 cosV sinhU + k_1 cos2V sinh2U + k_2 cos3V sinh3U$$

$$y = V + k_1 sinV coshU + k_2 sin2V cosh2V + k_2 sin3V cosh3V$$

The value of V is selected to be $\frac{\pi}{2} + \theta$, where θ is a variable and the value of x and y are calculated by sweeping the

variable U from 0 to a point where the slope of the curve becomes vertical. The geometry is controlled by 4 variables: θ , k_0 , k_1 and k_2 . The variables are generally chosen such that $k_0 > k_1 > k_2$. The geometry is more compact than Chang but harder to construct as the variables are chosen arbitrarily and the wrong combination of variables make the geometry go out of proportion.

III. ELECTRIC FIELD ANALYSIS

Electric breakdown in vacuum can take place either due to field emission or thermionic emission. The former causes electrostatically induced electrons to be emitted from the surface and the latter causes thermally charge carriers to flow over a potential barrier. While both field and thermionic emission can take place between the open contacts of FMS, only field emission is affected by the magnitude of electric field between the contacts. High electrostatic can result due to contaminants on the contact surface or change in the structure of the contacts due to deformation, friction and wear experienced by the contacts during the operation of FMS. Having a geometry that minimizes the electric field in the gap between the contacts can reduce the possibility of a breakdown when the contacts are open.

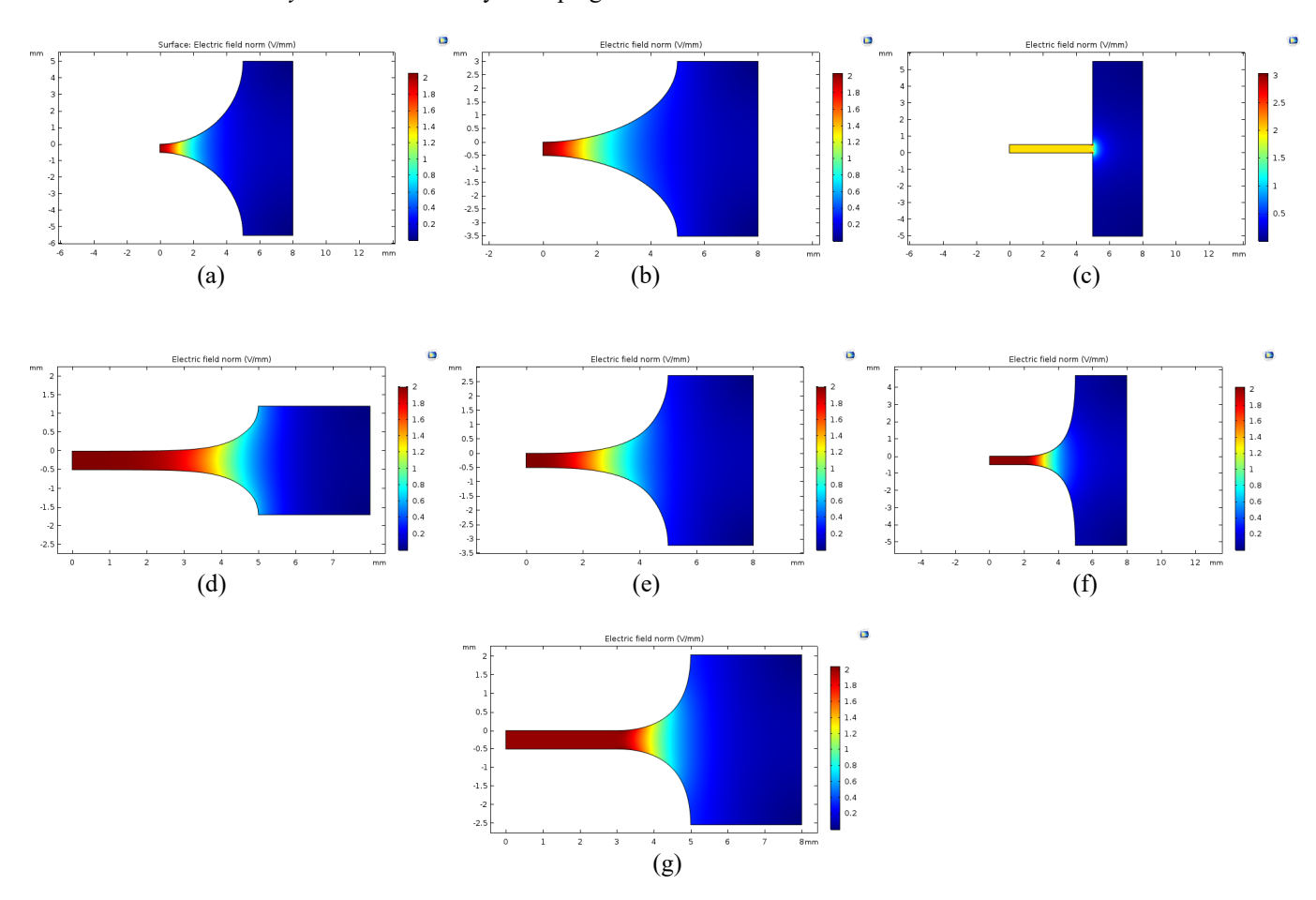


Fig. 2. Finite Element Result of Normalized Electric Field Distribution for contacts with 5mm base radius (a) Spherical, (b) Elliptical h=3 mm, (c) Flat h=5 mm, d) Rogowski $\phi=360^\circ$, (e) Bruce $\alpha=50^\circ$ Contact, (f) Chang k=0.2, (g) Ernst $k_1=0.3$, $k_2=k_3=10^{-4}$.

The electric field is modelled using a finite element model with 0.5 mm separation between the contacts for all geometries. All contacts have a circular base with radius of 5 mm. Since the electric contacts are symmetrical in two axes, a 2D axisymmetric model is used. The medium between the contacts is vacuum. The top contact is given a potential of 1 V and the bottom contact is grounded. The normalized electric field, i.e. the electric field vector normal to the surface, is plotted along the surface of the 1 V contact. The maximum electric field along the surface of the contact is tabulated. If the electric field is completely uniform, the normalized electric field will have a maximum value of 2 V/mm. The normalized electric field in the gap between the contacts for different geometries is shown in Fig. 2.

A) Spherical, Elliptical and Flat Geometry

Fig. 3 shows the variation of normalized electric field along the surface of the contact for circular, elliptical and flat contacts. It is seen that elliptical and flat geometries have lower electric field than circular geometry at the centre (0 mm in the x-axis). However, flat contacts have high electric field at the edges of the contact, which make them unsuitable as contacts of FMS. The peak electric field along the contact surface for these geometries are shown in Table I.

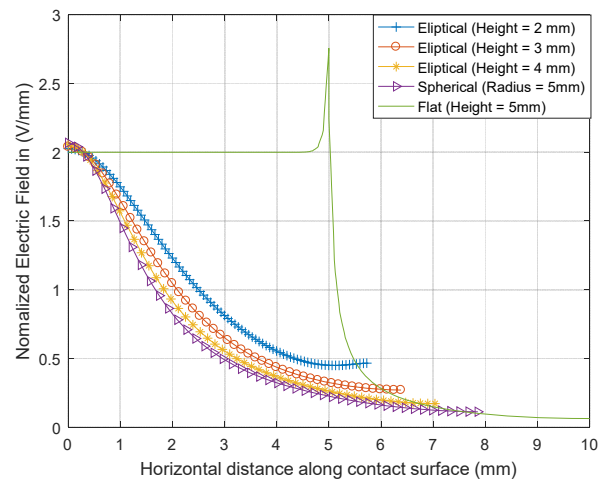


Fig. 3. Variation of Normalized Electric Field along surface for Spherical, Flat and Elliptical geometries.

 $TABLE\ I$ Peak Electric Field of Spherical, Flat and Elliptical Contacts (Radius = 5 mm)

Contact Geometry	Peak Electric Field (V/mm)
Spherical	2.0685
Flat	2.7577
Elliptical ($h = 2 \text{ mm}$)	2.0271
Elliptical ($h = 3 \text{ mm}$)	2.0406
Elliptical ($h = 4 \text{ mm}$)	2.0544

B) Rogowski and Bruce Geometry

Fig. 4 shows the variation of normalized electric field along the surface of the contact for different Rogowski geometries. Rogowski geometries with $\phi = 270^{\circ}$, 360° , 450° and 540° have a lower peak electric field than spherical geometry. The peak electric fields are shown in Table II.

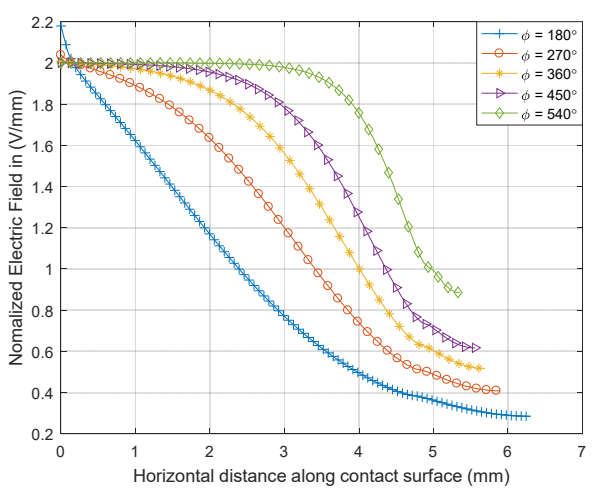


Fig. 4. Variation of Normalized Electric Field along surface for different Rogowski geometries.

 $TABLE\ II$ $P_{EAK}\ Electric\ Field\ of\ Rogowski\ Contacts\ (Radius=5\ mm)$

Contact Geometry	Peak Electric Field (V/mm)
$\phi = 180^{\circ}$	2.1790
$\phi = 270^{\circ}$	2.0380
$\phi = 360^{\circ}$	2.0081
$\phi = 450^{\circ}$	2.0017
$\phi = 540^{\circ}$	2.0000

Fig. 5 shows the variation of normalized electric field along the surface of the contact for different Bruce geometries. All the Bruce geometries shown have a lower peak electric field than spherical geometry. The peak electric fields are shown in Table III.

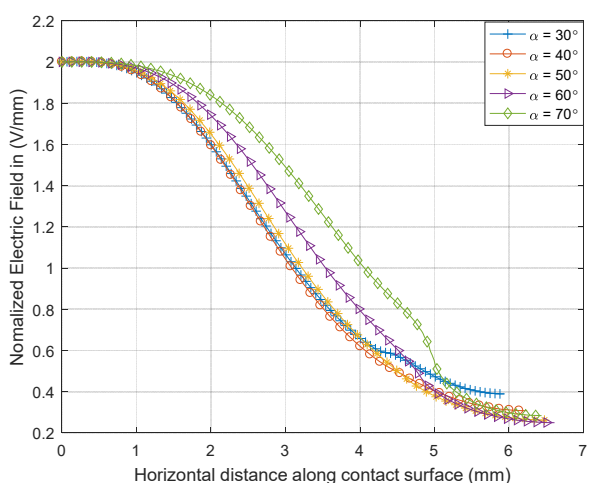


Fig. 5. Variation of Normalized Electric Field along surface for different Bruce geometries.

TABLE III

PEAK ELECTRIC FIELD OF BRUCE CONTACTS (RADIUS = 5 MM)

TEAR ELECTRIC FIELD OF BRUCE CONTACTS (RADIUS – 3 MM)	
Contact Geometry	Peak Electric Field (V/mm)
$\alpha = 30^{\circ}$	2.0023
$\alpha = 40^{\circ}$	2.0023
$\alpha = 50^{\circ}$	2.0019
$\alpha = 60^{\circ}$	2.0013
$\alpha = 70^{\circ}$	2.0007

C) Chang and Ernst Geometry

Fig. 6 shows the variation of normalized electric field along the surface of the contact for different Chang geometries. Although the electric field near the center of the geometry is uniform, field enhancement at the edges can lead to higher peak electric fields. Chang geometries with $k=0.2,\,0.3$ and 0.4 have a lower peak electric field than spherical geometry. The peak electric fields are shown in Table IV.

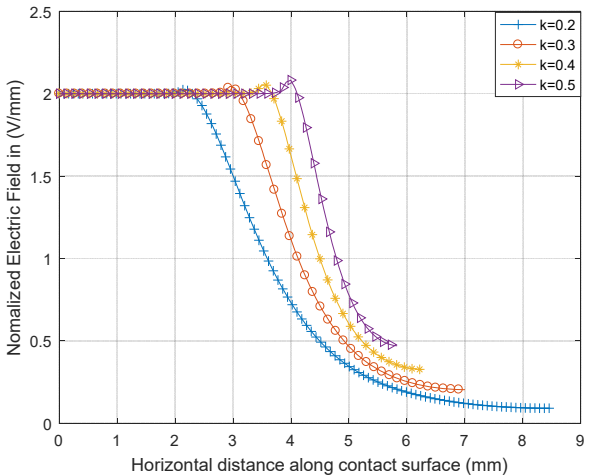


Fig. 6. Variation of Normalized Electric Field along surface for different Chang geometries.

 $TABLE\ IV$ Peak Electric Field of Chang Contacts (Radius = 5 mm)

Contact Geometry	Peak Electric Field (V/mm)
k = 0.2	2.0276
k = 0.3	2.0438
k = 0.4	2.0535
k = 0.5	2.0821

Fig. 7 shows the variation of normalized electric field along the surface of the contact for different Ernst geometries. Although the electric field near the center of the geometry is uniform, field enhancement at the edges can lead to higher peak electric fields. All the Ernst geometries shown in Table V have a lower peak electric field than spherical geometry.

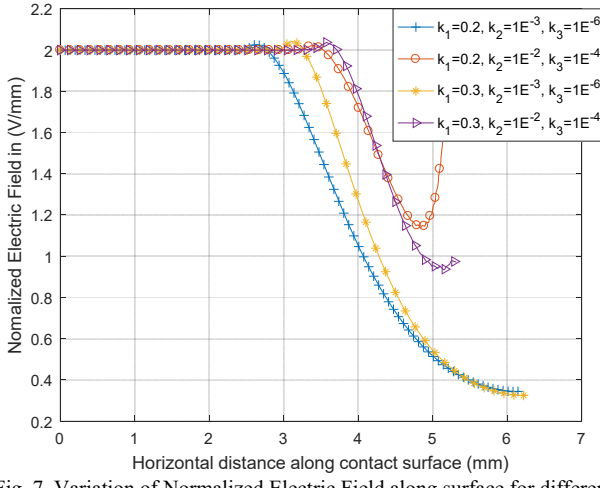


Fig. 7. Variation of Normalized Electric Field along surface for different Ernst geometries.

 $TABLE\ V$ Peak Electric Field of Ernst Contacts (Radius = 5 mm)

Contact Geometry	Peak Electric Field
	(V/mm)
$k_1 = 0.2, k_2 = 10^{-3}, k_3 = 10^{-6}$	2.0271
$k_1 = 0.2, k_2 = 10^{-2}, k_3 = 10^{-4}$	2.0218
$k_1 = 0.3, k_2 = 10^{-3}, k_3 = 10^{-6}$	2.0432
$k_1 = 0.3, k_2 = 10^{-2}, k_3 = 10^{-4}$	2.0376

IV. CONTACT RESISTANCE MEASURMENT

The electrical resistance of the contact geometries are measured experimentally. The experimental setup is shown in Figure 8.







Fig. 8. Picture of the Contact Experiment Setup (top left); CAD rendering of contact experiment with parts labelled (top right); Close up view of electric contacts showing banana plugs (bottom).

The setup consists of a six-way cross, which is a spherical chamber with ConFlat vacuum flanges at the six ends (top, bottom, front, back, left and right). On two opposite flanges, a feedthrough and a linear motion actuator are attached. Electric contacts are bolted to the copper feedthrough and a copper rod which is attached to the linear motion actuator through a load cell and a vibration mount. The force between the contacts is adjusted by manually rotating the actuator, which will press one contact onto the other. The load cell will measure the force between the contacts and the vibration mount is used to reduce the spring constant of the system. This allows the force between the contacts to be adjusted with an accuracy of +/-1 N. The measurements taken inside the chamber, such as force and the electric contact resistance are read outside the chamber through a multipin feedthrough. The chamber is evacuated using a pump and the measurements are taken at a maximum pressure of 10⁻³ mbar.



Fig. 9. Contact bolted to linear motion actuator

The design of contacts used in the experiment is shown in Fig. 10. All the contacts are made of high-purity 101 copper and are machined in a CNC mill. Copper is chosen due to its high conductivity and relative ease of obtaining the material (compared to actual contact materials like AgWC) for experimental purposes. All the contacts have a circular base with radius 5 mm. They are mounted on a 4 mm thick circular plate of 25 mm diameter. The plate has countersunk holes that allow the contact to be bolted to the feedthroughs without the bolt heads protruding. All the tested contacts have similar volume with 11% difference in volume between contact with the highest and lowest volume. So the difference in contact resistance between different geometries is mostly due to constriction resistance and not bulk resistance.



Fig. 10. CAD model of electric contact with parts labelled (left); Machined Rogowski contacts ($\phi = 3\pi$) (right).

Direct current is passed through the contacts using a fully programmable Magna Power TS Series power supply. The copper conductors to which the contacts are bolted have a hole through which banana plugs are inserted. The voltage drop between these terminals divided by the current is considered the resistance of the contacts for this experiment. The contacts are cleaned to remove any contaminants on its surface. The

resistance is measured at currents of 5, 10, 15, 20 and 25 A as a function of force by adjusting the force between the contacts from 5 N to 200 N. Since the currents are fairly low passed for a short duration (less than 1 minute), any effect on contact resistance due to Joule heating is minimized. Fig. 11 shows the contacts' resistance as a function of force for different contact geometries.

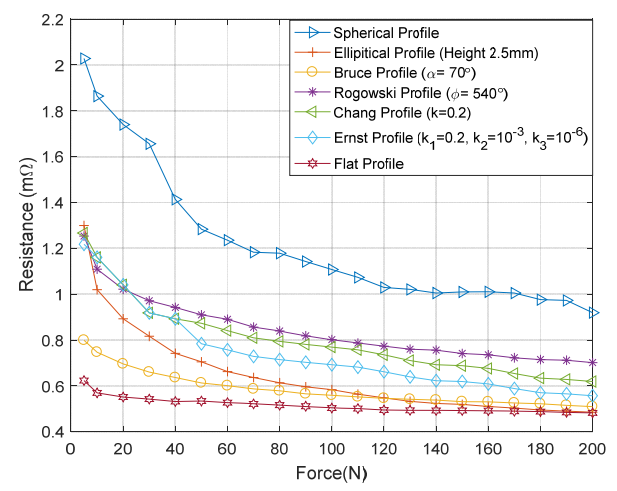


Fig. 11. Contact Resistance vs Force for different contact geometries.

The contact resistance has 3 components: bulk resistance, constriction resistance and film resistance [17]. At low loads, the film resistance will dominate as the oxide films, that have higher resistance than copper, are in contact. As the load is increased, the constriction resistance dominates as the number of a-spots increases. At high loads, the bulk resistance of the contacts will dominate as the real area of contact is very close to the nominal area of contact. In Fig. 6, the difference in volume between different geometries is 11% between the geometry with highest volume (flat) and lowest volume (Ernst). So the difference in contact resistance between different geometries cannot be due to the difference in bulk resistance.

It can be seen that spherical contacts, which are currently used in the FMS based on AMA, have the highest resistance and flat contacts have the lowest resistance. However, flat contacts have high electric field at their edges which make them unsuitable as contacts of the FMS. Optimized contact geometries such as Bruce, Rogowski, Ernst and Chang have low contact resistance as well as uniform electric field, which make them very suitable as contacts of a FMS. While contacts with higher nominal area of contact are generally observed to have lower resistance than contacts with lower nominal area, this is not true for elliptical contacts, which have lower contact resistance despite having lower nominal area of contact than Rogowski and Chang profiles. This could be due to the contact being slightly misaligned when placed in the experimental setup, which may have increased its nominal area of contact. Also, the surface roughness of the contacts have not been measured which could have caused elliptical contacts to have lower than expected resistance.

V. CONCLUSIONS AND FUTURE WORK

The electric contacts of FMS should have a geometry that results in low power loss when closed and uniform electric field when open. Different contact geometries such as Elliptical, Bruce, Rogowski, Ernst and Chang are explored to be used in proposed FMS. Finite element models show that optimized contact geometries have more uniform electric field that spherical geometry. Experimental results show that optimized geometries have upto 40% lower contact resistance than spherical geometry. Further research needs to be done on the effect of surface roughness on the contact resistance. The effect on electric contact material also has a significant effect on the performance on FMS and needs to be explored. The long term performance of contacts with proposed geometries also needs to be investigated.

VI. ACKNOWLEDGMENTS

This research was supported in part by the National Science Foundation (NSF) through the grant 1700887. The authors would also like to thank M. Steurer from the Center of Advanced Power Systems (CAPS), Florida State University, for his expert advice and great discussions.

VII. REFERENCES

- Alvin, Tan GM, Izham Z. Abidin, H. Hashim. "Changes in fault current levels due to renewable embedded generation in a distribution network." *IEEE Conference on Clean Energy and Technology (CEAT)*, 2013.
- [2] T. M. Masaud and R. D. Mistry, "Fault current contribution of Renewable Distributed Generation: An overview and key issues," 2016 IEEE Conference on Technologies for Sustainability (SusTech), Phoenix, AZ, 2016, pp. 229-234.
- [3] A. Shukla, G. D. Demetriades, "A survey on hybrid circuit-breaker topologies," *IEEE Transactions on Power Delivery*, 30(2), 627-641, 2015.
- [4] M. Steurer, K. Fröhlich, W. Holaus, K. Kaltenegger, "A novel hybrid current-limiting circuit breaker for medium voltage: principle and test results", *IEEE transactions on power delivery*, 18(2), 460-467, 2003.
- [5] C. Peng, I. Husain, A.Q. Huang, "Evaluation of design variables in Thompson coil based operating mechanisms for ultra-fast opening in

- hybrid AC and DC circuit breakers", *IEEE Applied Power Electronics Conference and Exposition (APEC)*, pp 2325-2332, Mar. 2015
- [6] L. Graber, S. Smith, D. Soto, I. Novak, J. Owens, M. Steurer, "A new class of high speed disconnect wsitch based on piezo electric actuators", *IEEE Electric Ship Technologies Symposium (ESTS)*, pp 307-312, Jun. 2015.
- [7] L. Graber, C. Widener, C. Smith, M. Steurer "Thermal-Electrical Study of an Ultra-fast Disconnect Switch with a Piezoelectric Actuator.", COMSOL Conference, 2014.
- [8] L. Graber, C. Widener, S. Smith, M. Steurer, "Ultrafast Electromechanical Disconnect Switch," US Patent application 15/214.015, 2016.
- [9] M. Bosworth, D. Soto, R. Agarwal, M. Steurer, T. Damle and L. Graber, "High speed disconnect switch with piezoelectric actuator for medium voltage direct current grids," 2017 IEEE Electric Ship Technologies Symposium (ESTS), Arlington, VA, 2017, pp. 419-423.
- [10] N. G. Trinh, "Electrode Design for Testing in Uniform Field Gaps," in *IEEE Transactions on Power Apparatus and Systems*, vol. PAS-99, no. 3, pp. 1235-1242, May 1980.
- [11] W. Rogowski, "Die elektrische Festigkeit am Rande des Plattenkondensators. Ein Beitrag zur Theorie der Funkenstrecken um Durchfuhrungen", Archiv fur Electrotechnik, Vol. 12, No. 1, 1923, pp. 1-15.
- [12] F.M. Bruce, "Calibration of uniform-field spark-gaps for high-voltage measurement at power frequencies", *Journal of IEE*, Vol. 94, Part II, 1947, pp. 138-149.
- [13] G. C. Lim, T. Damle and L. Graber, "Optimized contact geometries for high speed disconnect switches," 2017 IEEE Conference on Electrical Insulation and Dielectric Phenomenon (CEIDP), Fort Worth, TX, 2017, pp. 537-542.
- [14] S. S. Anufrik, A. P. Volodenkov and K. F. Znosko, "Selection of electrodes profile for excimer lasers," 2010 10th International Conference on Laser and Fiber-Optical Networks Modeling, Sevastopol, 2010, pp. 198-200.
- [15] I. Leyva and, J. M. Guerra, "A compacted Ernst-electrodes profile for pulsed high-pressure lasers," *Measurement Science and Technology*, 10, pp.N1-N2, 1999.
- [16] T. Y. Chang, 'Improved uniform-field-electrode profiles for TEA lasers," Review of Scientific Instruments, vol. 44, pp. 405-407, Apr. 1973
- [17] Y. Zeroukhi, E. Napieralska Juszczak, K. Komeza, F. Morganti, and G.Vega, and S. Wiak, "Dependence of the contact resistance on the design of stranded conductor," *Sensors*, vol. 14, no. 8, pp. 13925–13942, May 2014.